Defect Engineering: Tuning the Porosity and Composition of the Metal-Organic Framework UiO-66 via Modulated Synthesis

(Article begins on next page)

19 September 2024

Defect Engineering: Tuning the Porosity and Composition of the Metal-Organic Framework UiO-66 via Modulated Synthesis

Greig C. Shearer, Sachin Chavan, Silvia Bordiga, Stian Svelle, Unni Olsbye, Karl Petter Lillerud.

Defect Engineering: Tuning the Porosity and Composition of the Metal-Organic Framework UiO-66 via Modulated Synthesis

Greig C. Shearer,† Sachin Chavan,† Silvia Bordiga,†,‡ Stian Svelle,† Unni Olsbye, Karl Petter Lillerud*.†

† Department of Chemistry, University of Oslo, P.O. Box 1033, N-0315 Oslo, Norway

‡ Department of Chemistry, NIS and INSTM Reference Centre, University of Torino, Via G. Quarello 15, 10135 Torino

ABSTRACT: Presented in this paper is a deep investigation into the defect chemistry of UiO-66 when synthesized in the presence of monocarboxylic acid modulators under the most commonly employed conditions. We unequivocally demonstrate that missing cluster defects are the predominant defect, and that their concentration (and thus the porosity and composition of the material) can be tuned to a remarkable extent by altering the concentration and/or acidity of the modulator. Finally, we attempt to rationalize these observations by speculating on the underlying solution chemistry.

INTRODUCTION

Metal-organic frameworks (MOFs) with hexanuclear Zr_6 inorganic cornerstones ("Zr_6 MOFs")[1] have come to recent prevalence in the literature.[2-27] Their popularity can be attributed to their superior stability[2, 7-10, 19, 20, 23, 25] and the ease at which a wide range of functionalities can be introduced.[28-42] UiO-66 ($Zr_6(OH)_4O_4(BDC)_6$, BDC = Benzene-1,4-dicarboxylate) was the first Zr_6 MOF to be reported,[9] and is by far the most widely studied.

In 2011, Behrens and co-workers showed that relatively large and monodisperse UiO-66 crystals could be obtained by adding monocarboxylic acid "modulators" to the synthesis mixture.[43] Variants of this synthesis method have since been popularized in the literature.[30, 34, 39, 44-48] However, recent work has shown that modulated synthesis routes promote the formation of defects,[24, 49-58] which can have a profound (and in some cases, positive) impact on the stability,[59-62] reactivity,[55] porosity,[28, 58, 59] and thermomechanical behavior[52] of UiO-66. Affording control over the defects thus allows MOF chemists to fine-tune the properties of the material and potentially improve its performance in various applications. Indeed, defects have

been shown to have a positive influence on UiO-66's catalytic,[56, 63-67] adsorption,[58, 62, 68, 69] decontamination,[70-72] and proton conductivity[51] capabilities.

Two types of defects have been proposed to exist in the UiO-66 framework: "missing linker defects"[33, 49, 54-58, 63, 64, 68, 70, 72-77] and "missing cluster defects"[24, 50-52, 77, 78] (see **Figure 1** below). Missing cluster defects were recently discovered by Goodwin and co-workers.[50] In a highly convincing study, they demonstrated that using formic acid as a modulator promotes the formation of a material in which missing cluster defects exist in correlated nanoregions of the **reo** topology. In the defective **reo** phase, the clusters have reduced linker connectivity (8) with respect to ideal UiO-66 (12). This results in a charge imbalance which the authors assume to be compensated by formate anions (originating from the formic acid modulator), allowing the clusters to maintain the familiar $Zr_6(OH)_6O_4(CO_2)_{12}$ geometry. A visual depiction of the above (albeit with trifluoroacetate as the defect compensating ligand) is shown on the left-hand side of **Figure 1**.

The first detailed investigation into missing linker defects was performed by the Zhou group.[58] They showed

reo phase
Missing Cluster Defect

$-1 * \left[\ \right]^{12-}$

$Zr_6O_6(BDC)_{12}^{12-}$

Ideal UiO-66

$-8 * BDC^{2-}$

Missing Linker Defects

$3 \cdot Zr_6O_6(BDC)_4(O_2C\text{-}CF_3)_4$ $+12 * O_2C\text{-}CF_3^-$ $4 \cdot Zr_6O_6(BDC)_6$ $+16 * O_2C\text{-}CF_3^-$ $4 \cdot Zr_6O_6(BDC)_4(O_2C\text{-}CF_3)_4$
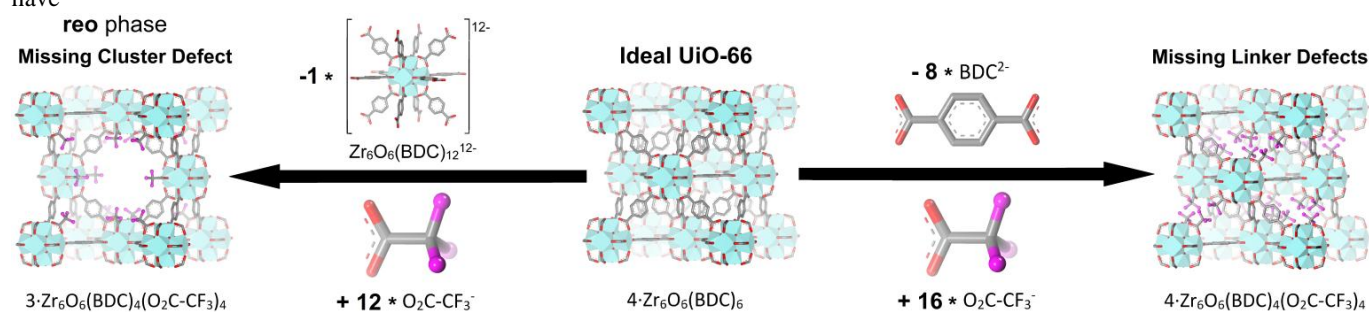
Figure 1. Illustration depicting the structural and compositional differences between the ideal UiO-66 unit cell and those with missing cluster/ missing linker defects. Trifluoroacetate ligands compensate for the defects in the examples above; however, the compensating ligand can vary depending on the modulator used during the MOF synthesis.

that the porosity of UiO-66 tends to increase as increasing amounts of acetic acid are used in the synthesis. Based on this observation, they concluded that acetic acid promotes the formation of missing linker defects by acting as the defect compensating ligand (as acetate). Similar conclusions were made by Vermoortele et al., who synthesized extremely defective UiO-66 samples using trifluoroacetic acid as a modulator.[56] A

hypothetical model of such a material is shown on the right-hand side of **Figure 1**.

The three studies discussed above each involved the use of a different monocarboxylic acid as modulator. It therefore occurred to us that the properties (particularly the acidity) of the modulator may have a strong and perhaps even logical influence on the nature and/or concentration of defects in the UiO-66 framework. This prompted us to perform a systematic in-

vestigation involving 15 UiO-66 syntheses in which only the concentration and/or acidity (pK_a) of the modulator was varied (see **Scheme 1**). In order to ensure that our study is as relevant as possible, all syntheses were performed under the most widely employed reaction conditions ($ZrCl_4$ as Zr^{4+} source, 1 : 1 linker : Zr ratio, DMF as solvent, crystallization temperature = 120 °C). All 15 samples were thoroughly characterized by PXRD, nitrogen sorption, dissolution/NMR, TGA-DSC, SEM/EDX, and ATR-IR.

Four of these techniques (PXRD, nitrogen adsorption, dissolution/NMR, and TGA) provide important information related to the concentration of defects in the samples, affording us the opportunity to demonstrate the incredible extent to which the defect concentration can be tuned. Moreover, quantitative data was extracted from the 4 techniques, allowing us to discover trends and unveil the nature of the defects. Our findings are further validated by comparing experimentally obtained nitrogen adsorption isotherms with those simulated from hypothetical defective UiO-66 structural models. Finally, we attempt to rationalize our conclusions by speculating on the underlying solution chemistry.

EXPERIMENTAL DETAILS

The compositions of the 15 UiO-66 synthesis mixtures are shown schematically in **Scheme 1** The synthesis mixtures were prepared in volumetric flasks. Once all reagents had dissolved, the flasks were loosely capped and transferred to an oven set to 120 °C. After 72 hours of reaction, the resulting microcrystalline powders were thoroughly washed and activated. Full details of the synthesis, washing, and activation procedures are provided in the SI.

Detailed descriptions of the characterization methods (PXRD, nitrogen sorption, dissolution/NMR, TGA-DSC, SEM, EDX, and ATR-IR), simulations (PXRD and nitrogen adsorption), and quantitative analysis methods are provided in the supporting information (hereafter referred to as the "SI").

Scheme 1. a) The similarities and b) The differences between the compositions of the 15 UiO-66 synthesis mixtures. Quantities are provided in molar equivalents (eq.) so that the molar ratios between the reagents can be easily discerned.
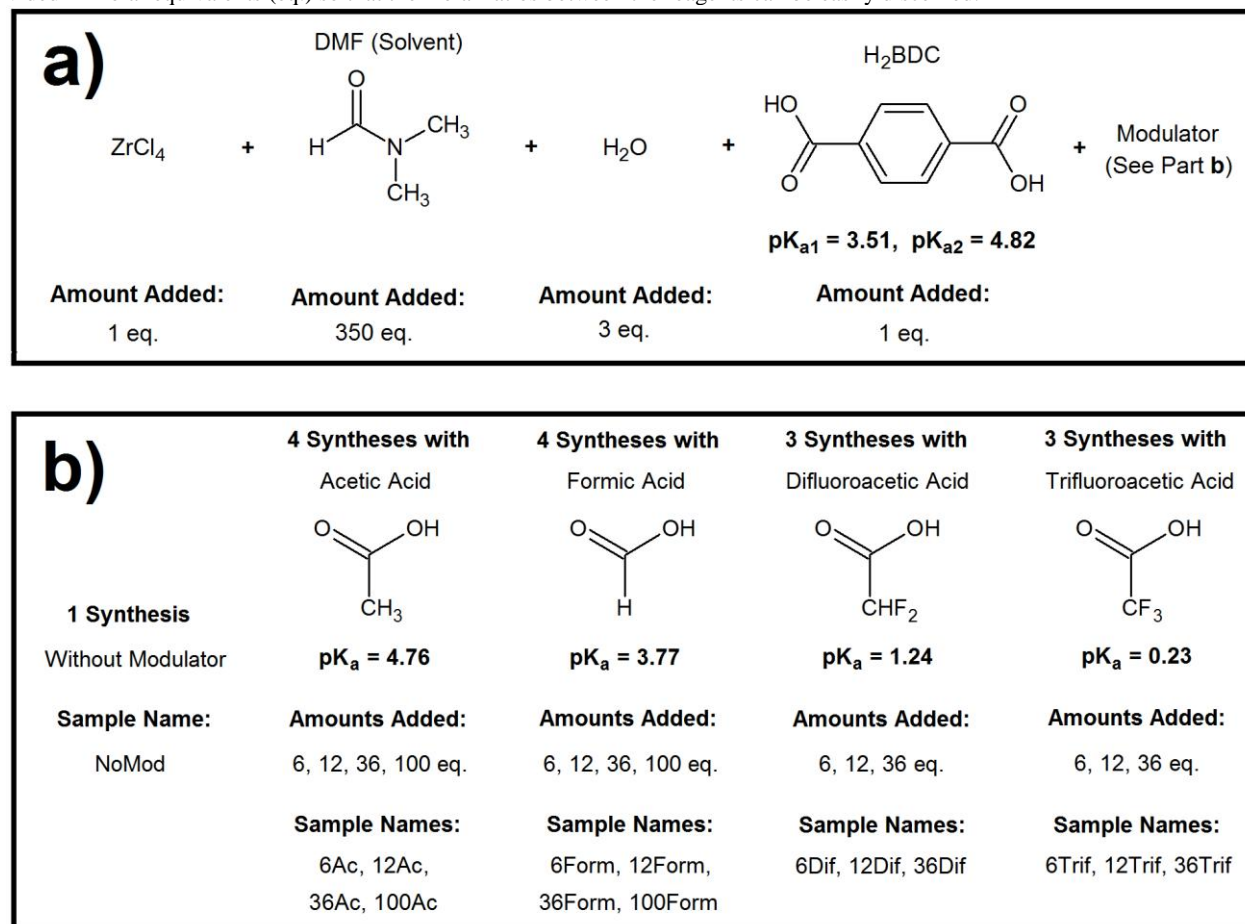
RESULTS AND DISCUSSION

Nitrogen Sorption Isotherms

The nitrogen sorption isotherms obtained on all 15 UiO-66 samples at 77K are shown in **Figure 2** below. As can be seen, the nitrogen uptake capacity (and thus, porosity) of the samples varies enormously depending on the acidity and concentration of the modulator used in the MOF synthesis. Of even greater interest is the observation of two remarkably conspicuous trends:

1) The nitrogen uptake (and thus, porosity) of the samples systematically increases as increasing amounts of modulator were added to the synthesis mixture. This observation holds for all 4 modulators.

2) The nitrogen uptake (and thus, porosity) of the samples systematically increases as the acidity/pK_a of the modulator was increased/decreased.

These two trends exemplify the astounding extent to which the porosity of UiO-66 may be tuned via judicious use of modulator. The only outlier is 6Trif (red curve in rightmost plot). Based on the 2nd trend outlined above, one would have expected it to adsorb more nitrogen than 6Dif (red curve in second plot from the right). The surprisingly low porosity of 6Trif can be attributed to the fact that it contains an impurity phase: MIL-140, another zirconium terephthalate MOF which is considerably denser than UiO-66. Evidence for the presence of this impurity is presented in **Section 5.14** of the SI.

Another important observation is that NoMod (black curve in all 4 plots) is considerably less porous than all other samples. In fact, it is slightly less porous than ideal UiO-66, as determined by comparing its nitrogen adsorption isotherm with that simulated from a defect-free UiO-66 structural model (see in **Section 5.5.1** of the SI). As one can see, using just 6 molar equivalents of any of the 4 modulators (red curves) leads to a substantial increase in porosity.

Quantitative data was extracted from the isotherms by calculating the **BET surface areas** of the samples (see **Section 3.3** of the SI for method and **Table S15** for the numerical values). **Figure 3** is the graph obtained when the **BET surface areas** of all 15 samples are plotted against the molar equivalents of modulator added to their syntheses:
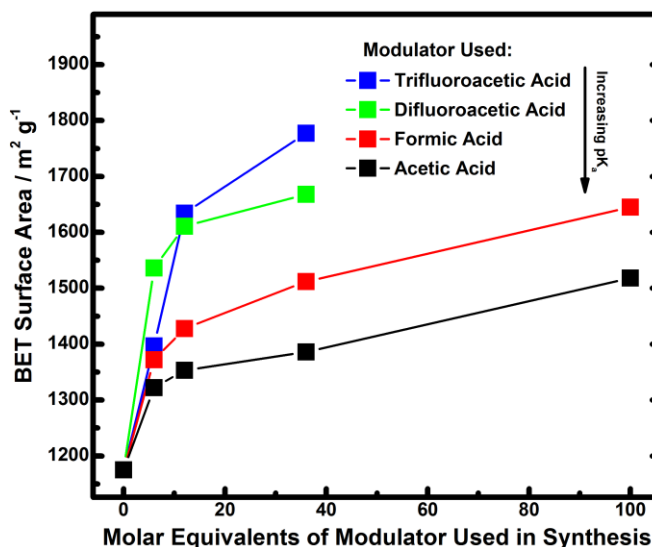

Figure 3. Graph obtained when the BET surface areas of the 15 UiO-66 samples (see **Table S15**) are plotted against the molar equivalents of modulator added to their syntheses.

As can be seen, the **BET surface areas** of the samples vary significantly, ranging from 1175 m^2g^{-1} (NoMod) to 1777 m^2g^{-1} (36Trif), which is one of the highest BET surface areas ever reported for UiO-66 (the current record is 1890 m^2g^{-1}).[79] More importantly, the trends in porosity (now quantitatively described by the **BET surface area**) are the same as those qualitatively observed in **Figure 2**, including the observation that 6Trif (blue data point at **x = 6**) is the only outlier.
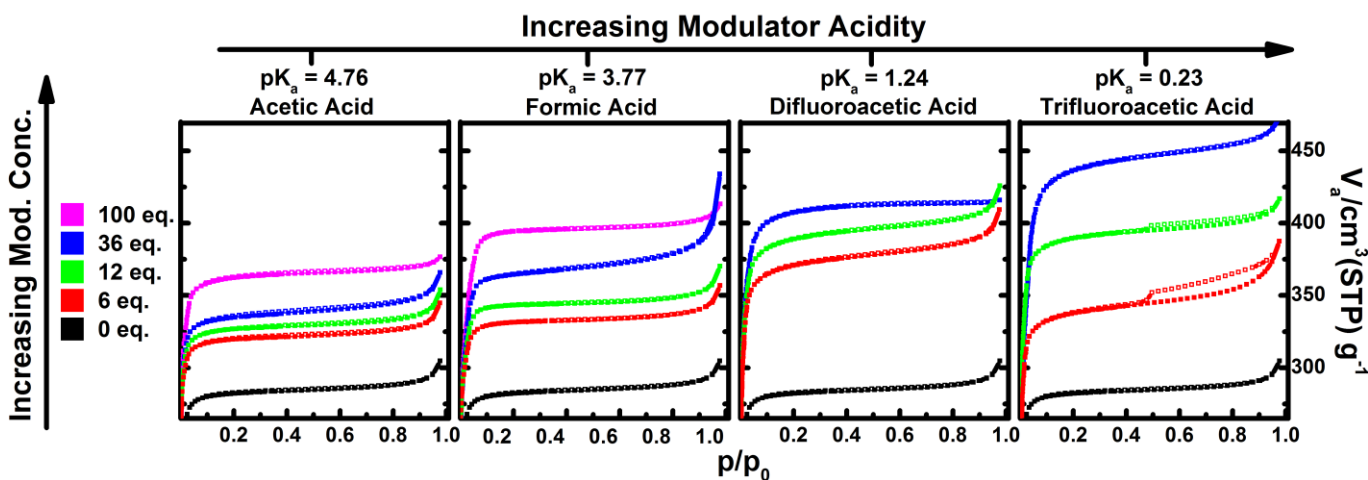

Figure 2. Nitrogen adsorption isotherms obtained on all 15 UiO-66 samples at 77 K. Adsorption represented by filled squares, desorption by open squares. The same y-scale is applied to all four plots.

PXRD

When compared over a relatively wide 2θ range (2-50°), the differences between the PXRD patterns obtained on the 15 samples are not immediately obvious (see **Figure S10** in the

SI). However, if one looks at the 2θ region around the (111) (the strongest, and ideally, the first) reflection of UiO-66 (appearing at *ca.* 7.4 ° 2θ), interesting trends emerge. This region (2-12° 2θ) is emphasized in **Figure 4**.

As one can see, most of the patterns contain a very broad peak spanning a 2θ range of *ca.* 2-7°. This peak cannot be attributed to the UiO-66 phase. The assignment of this peak (hereafter simply referred to as the "broad peak") is discussed in **Section 5.1.2.** of the SI, where we confidently assign it to **reo** nanoregions which are even smaller than those previously observed by Goodwin and co-workers.[50] As shown in **Figure 1**, the **reo** phase can be thought of as UiO-66 with one quarter of its clusters missing. For this reason, the terms "missing cluster defects" and "**reo** phase/nanodomains" are used interchangeably herein.

In their inspiring study, Goodwin and co-workers demonstrated that the intensity of the **reo** reflections (relative to those of UiO-66) is correlated with the concentration of missing cluster defects in the sample. With this in mind, we note 2 qualitative trends regarding the intensity of the broad peak when observing **Figure 4**:

1) It systematically increases as increasing amounts of modulator were added to the synthesis mixture. This observation holds for all 4 modulators.

2) It systematically increases as the acidity/pK$_a$ of the modulator was increased/decreased.

In order to quantitatively scrutinize these perceived trends, we calculated the relative intensity of the broad peak ($Rel(I)_{B.P.}$) in each of the PXRD patterns (see **Section 3.1** of SI for method). **Figure 5** is the graph obtained when the $Rel(I)_{B.P.}$ values of all 15 samples (see **Table S4**) are plotted against the molar equivalents of modulator added to their syntheses:
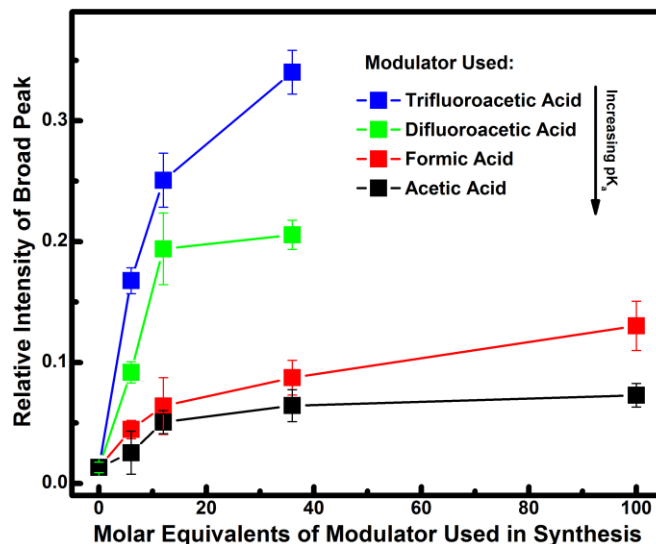
Figure 5. Graph obtained when the $Rel(I)_{B.P.}$ values (see **Table S4**), are plotted against the molar equivalents of modulator added to the UiO-66 synthesis mixture.

As can be seen, the trends in $Rel(I)_{B.P.}$ (and thus, the concentration of missing cluster defects in the UiO-66 framework) are the same as those qualitatively observed upon inspection of **Figure 4**, with absolutely no outliers.
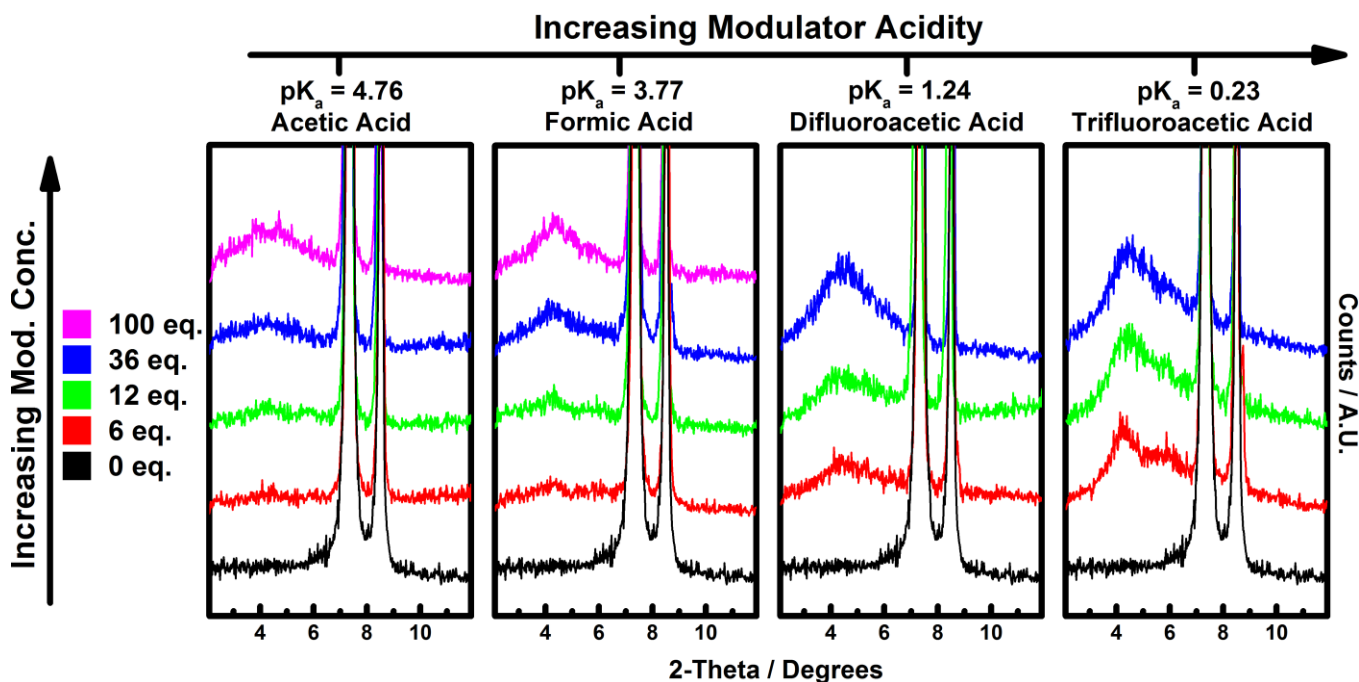
Figure 4. Low angle (2-12° 2θ) region of the PXRD patterns obtained on all 15 UiO-66 samples. Samples were activated (i.e. desolvated) prior to measurement (see **Section 1.1** of the SI for details). The same y-scale is applied to all four plots.

The Identity of the Defect Compensating Ligands

As demonstrated in **Figure 1**, terminal ligands are required to compensate for the defects in the UiO-66 framework (a role fulfilled by trifluoroacetate in the figure). In order to fully understand the defect chemistry of our samples, we need to ascertain the identity of the defect compensating ligands. To this end, three possibilities were investigated based on observations and/or speculations in previous studies; chloride,[49, 56, 59, 69, 76, 77, 80] OH^-/H_2O,[33, 51, 64, 66, 68, 70, 71, 73, 74, 81, 82] and monocarboxylates[49-58] (i.e. deprotonated modulator molecules such as trifluoroacetate, see **Figure 1**). However, chloride and hydroxide were quickly ruled out on the basis of EDX (**Figure S54**) and ATR-IR (**Figure S55**) results, respectively.

With the other two possibilities eliminated, dissolution/NMR (both ^{1}H and ^{19}F) was used to investigate the possibility that monocarboxylates compensate for the defects in our samples.

Dissolution/NMR Spectroscopy

The dissolution/NMR technique involves the dissolution (a.k.a. digestion or disassembly) of the MOF in a deuterated digestion medium. The organic components (e.g. linker, modulator, pore-filling solvent) can then be identified and quantified (as a molar ratio with other organic components) by liquid NMR spectroscopy.

As a representative example of the results obtained in this work, the ^{1}H NMR spectra recorded on the acetic acid modulated samples after digestion in 1M NaOH (in D_2O) are displayed in **Figure 6**. The spectrum obtained on NoMod is included for comparison. See **Section 5.2.2** of the SI for equivalent figures and subsequent discussion of the results obtained on the formic, difluoroacetic, and trifluoroacetic acid modulated samples.

Looking at the full chemical shift range of the spectra, one can see that they are exceptionally clean. There are only 3 signals, which have been confidently assigned to BDC^{2-}, acetate, and formate on the figure. This is an early indication that monocarboxylates (both formate and acetate) do indeed compensate for the defects in these samples. However, it is of utmost importance to ascertain whether these species are actually incorporated into the UiO-66 framework or if they are simply occluded in the pores as free acids. To this end, the MOF washing and activation (i.e. desolvation) procedures are heavily scrutinized in **Section 5.2.1** of the SI, where we conclude that all free monocarboxylic acids (acetic, formic, difluoroacetic, or trifluoroacetic acid) were successfully removed by these treatments. We can therefore be very confident that all monocarboxylates detected after activation are indeed incorporated into the UiO-66 framework (as is the case in **Figure 6**).

With this in mind, let us return to the spectra presented in **Figure 6**, where one can see that the acetate signal systematically increases in intensity as increasing amounts of acetic acid were used in the synthesis. Equivalent trends are observed for the samples synthesized with the other 3 modulators under investigation (see **Section 5.2.2** of SI). Moreover, similar trends in the intensity of bands related to the modulator can (in some cases) be seen in ATR-IR spectra (see Figures **S56-S59**). Both dissolution/NMR and ATR-IR results therefore show that the extent of modulator incorporation is strongly correlated with the concentration of modulator in the UiO-66 synthesis solution.
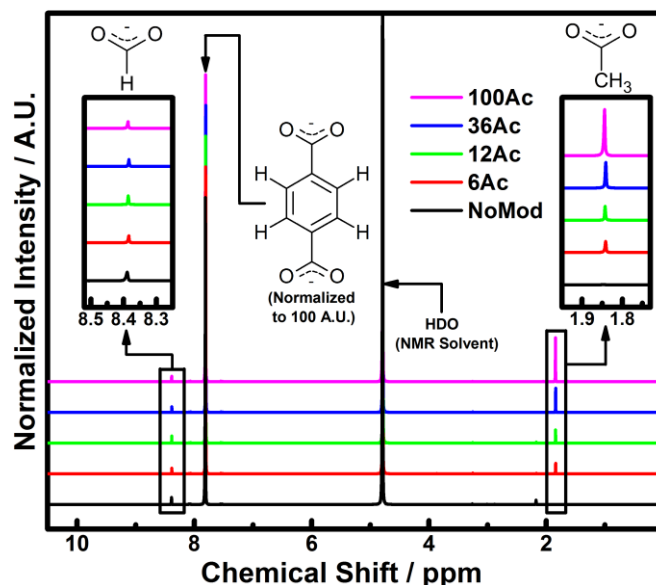
Figure 6. Dissolution/^{1}H NMR spectra obtained on the acetic acid modulated samples. NoMod is included for comparison. Samples were activated (i.e. desolvated) prior to measurement (see **Section 1.1** of SI for details).

A more surprising observation from **Figure 6** is that all 5 samples contain formate, despite the fact that no formic acid was added to their synthesis mixtures. The acetic acid modulated samples are certainly not unique in this respect - formate is in fact present in the spectra obtained on all 15 samples. This is not too surprising for the formic acid modulated samples (6Form, 12Form, 36Form, and 100Form). However, intentionally added modulator cannot account for the formate observed in the 11 non formic acid modulated samples. The origin of this formate is discussed in **Section 5.2.1** of the SI, in which we conclude that it originates from formic acid generated by DMF hydrolysis during the MOF syntheses.

The discussion of our dissolution/NMR results has so far been limited to qualitative spectral comparisons; however, the real strength of the technique is that one can determine molar ratios between the MOF's organic components by integration. In this work, 3 different molar ratios were calculated (see **Section 3.2** of SI for methods):

1) The "intentionally added modulator to BDC molar ratio" i.e. the formate : BDC, acetate : BDC, difluoroacetate : BDC, and trifluoroacetate : BDC molar ratios in the formic, acetic, difluoroacetic, and trifluoroacetic acid modulated samples, respectively. Values are presented in **Table S12**.

2) The formate : BDC molar ratio in the *non-formic acid modulated* samples. Values are presented in **Table S13**.

3) The "total modulator to BDC ratio". This is the sum of 1) and 2) above. Values are presented in **Table S14**.

Following much discussion in **Section 5.2.3** of the SI, we concluded that the total modulator to BDC molar ratio, $\frac{\text{Tot. Mod.}}{\text{BDC}} m_R$ is the fairest ratio to use when comparing the materials. It is essentially a quantitative descriptor for the concentration of monocarboxylate terminated defects in the UiO-66 framework. **Figure 7** is the graph obtained when the

$\frac{\text{Tot. Mod.}}{\text{BDC}}\mathbf{m}_R$ values of all 15 samples are plotted against the molar equivalents of modulator added to their syntheses:

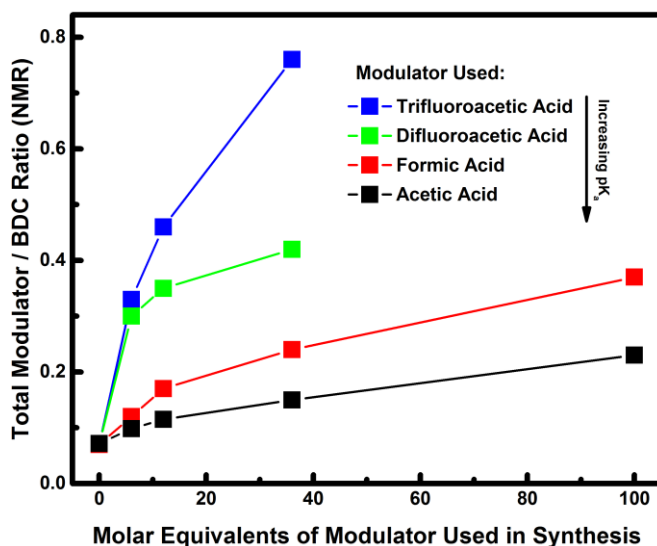**Figure 7.** Graph obtained when the total modulator to BDC molar ratios ($\frac{\text{Tot. Mod.}}{\text{BDC}}\mathbf{m}_R$, see **Table S14** in the SI) are plotted against the molar equivalents of modulator added to the UiO-66 synthesis mixture.

As can be seen, an enormous range of $\frac{\text{Tot. Mod.}}{\text{BDC}}\mathbf{m}_R$ values are observed in the samples. The most defective sample (36Trif) contains a huge amount of modulator; 0.76 molecules for every linker molecule. Of even greater interest is the observation of two very clear trends in the figure:

1) The total modulator to BDC ratio (and thus the concentration of monocarboxylate terminated defects in the UiO-66 framework) systematically increases as increasing amounts of modulator were added to the synthesis mixture. This observation holds for all 4 modulators.

2) The total modulator to BDC ratio (and thus the concentration of monocarboxylate terminated defects in the UiO-66 framework) systematically increases as the acidity/pK$_a$ of the modulator was increased/decreased.

TGA-DSC

All TGA-DSC results obtained in this work are qualitatively similar. As a representative example, the results obtained on the formic acid modulated samples are presented in **Figure 8**. The result obtained on NoMod is included for comparison. See **Section 5.6** of the SI for equivalent figures (and subsequent discussion) concerning the results obtained on the acetic, difluoroacetic, and trifluoroacetic acid modulated samples.
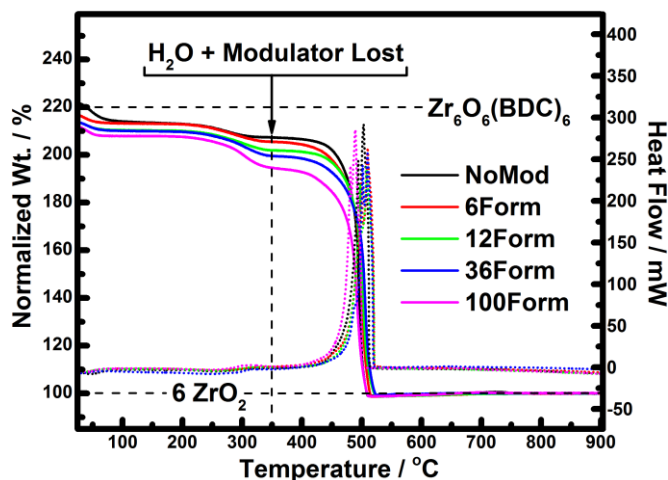

Figure 8. TGA-DSC results obtained on the formic acid modulated samples. NoMod is included for comparison. Samples were activated (i.e. desolvated) prior to measurement (see **Section 1.1** of SI for details). Solid curves, left axis - TGA trace (normalized such that end weight = 100%). Dotted curves, right axis – DSC signal.

Three well resolved weight losses are observed in the TGA traces (end weight normalized to 100 %). In accordance with previous studies, the losses are assigned to the following processes:

1) Adsorbate volatilization (in this case H$_2$O). Occurs over a temperature range of *ca*. 25-100 °C.

2) Removal of monocarboxylate ligands[52, 56] (in this case formate), and dehydroxylation of the Zr$_6$ cornerstones.[9, 75, 80, 83] These two weight loss events occur over a similar temperature range (*ca*. 200-350 °C) and are thus not well resolved from one another. Formate loss is accompanied by a small exothermic peak in the DSC signal.

3) Framework decomposition.[52, 56, 75] Occurs over a temperature range of *ca*. 390 – 525 °C and is accompanied by a very intense exothermic peak in the DSC signal.

The framework decomposition weight loss step involves the complete combustion of the BDC linkers. It is now well established that the magnitude of this weight loss (when normalized as above) is inversely correlated with the defectivity of the UiO-66 sample in question.[52, 56, 59, 75] This makes sense when one compares the compositions of the structures provided in **Figure 1**. Therein, one can see that ideal, defect free (and dehydroxylated) UiO-66 has a composition of **Zr$_6$O$_6$(BDC)$_6$**, where each Zr$_6$ formula unit contains 6 BDC linkers, meaning that (6 x 2) = **12** linkers are coordinated to each Zr$_6$ cluster. On the other hand, there are only 4 linkers per Zr$_6$ formula unit in either of the hypothetical defective structural models, meaning that (4 x 2) = **8** linkers are coordinated to their clusters. Both missing linker and missing cluster defects therefore introduce "linker deficiencies" to the UiO-66 framework. Given that the decomposition weight loss involves the loss of linkers, the magnitude of the weight loss is reduced when defects (and thus linker deficiencies) are present. However, it is ***impossible to distinguish*** between missing linker and missing cluster defects using TGA alone (see **Section 3.4.1.** of the SI for more on this).

With all of the above in mind, let us return our attention to **Figure 8**, where the theoretically expected weight loss for the decomposition of ideal (dehydroxylated) UiO-66, $Zr_6O_6(BDC)_6$ is represented by the vertical gap between the two horizontal dashed lines. In order to fairly compare the samples to this ideal, we need to pinpoint the stage at which everything except the BDC linkers has been lost (i.e. when the 2nd weight loss step is complete). This point is emphasized with a vertical dashed line on the figure (see **Section 3.4.4** in the SI for details of how this choice is made). Commencing from this point, one can see that the magnitude of the decomposition weight loss is significantly lower than that theoretically expected in all samples, indicating that they are linker deficient. More importantly, there is a clear trend among the samples: the magnitude of the decomposition weight loss systematically decreases (and thus the defectivity of the material increases) as increasing amounts of formic acid were added to the synthesis mixture. The same trend was observed for all samples except the acetic acid modulated materials (see discussion of **Figure 9** later).

In order to quantitatively compare the entire series of samples, we calculated the "number of linker deficiencies per Zr_6 formula unit" from the TGA traces obtained on each of the 15 samples. This is the value of x in the general molecular formula $Zr_6O_{6+x}(BDC)_{6-x}$, the assumed composition of the material immediately before the decomposition weight loss step commences. The value of x is correlated with the overall defectivity of the material and inversely correlated with the magnitude of the decomposition weight loss. A detailed description of the method used to calculate x is provided in **Section 3.4** of the SI. As an interesting aside, we have used the x values (in combination with the molar ratios obtained via dissolution/NMR) to attain very promising estimates for the overall (hydroxylated) composition of each of our samples. The method and results can be found in **Sections 3.5** and **5.8** of the SI, respectively.

Figure 9 is the graph obtained when the x values of all 15 samples (see **Table S24** in the SI) are plotted against the molar equivalents of modulator added to their syntheses. As can be seen, the samples differ widely in their defectivity. The most defective sample in the series is once again shown to be 36Trif, which contains **2** linker deficiencies per Zr_6 formula unit, meaning that there are $(6 - 2) = 4$ linkers in its average formula unit and only $(4 \times 2) = \underline{\textbf{8}}$ linkers coordinated to its average Zr_6 cluster. This is an astonishing level of defectivity considering that 12 linkers are coordinated to the cluster in the ideal material. More importantly, two clear trends are once again observed in the figure:

1) The number of linker deficiencies (and thus, the defectivity of the material) systematically increases as increasing amounts of modulator were added to the synthesis mixture. This observation holds for all modulators except acetic acid, where the number of linker deficiencies is nearly constant unless very large amounts of modulator (100 eq.) were used.

2) The number of linker deficiencies (and thus, the defectivity of the material) systematically increases as the acidity/pK_a of the modulator was increased/decreased.
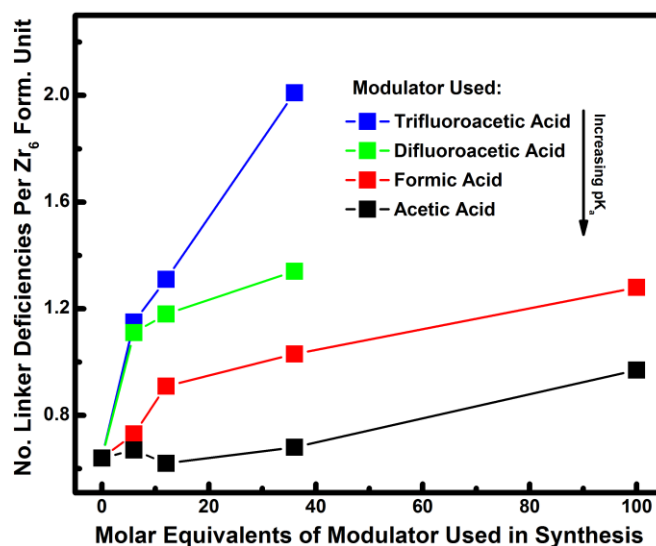

Figure 9. Graph obtained when the number of linker deficiencies per Zr_6 formula unit (x, see **Table S24** in the SI) are plotted against the molar equivalents of modulator added to the UiO-66 synthesis mixture.

Correlations - the Nature of the Defects

One may have noticed that the trends observed in **Figures 3**, **5**, **7**, and **9** are qualitatively rather similar. This suggests that the parameters plotted in the graphs are correlated, which makes sense given that all 4 parameters are essentially quantitative descriptors for the defectivity of the samples:

1) The **BET surface area** of UiO-66 has previously been shown to be correlated with its defectivity.[58, 59]

2) The relative intensity of the broad peak ($Rel(I)_{B.P.}$) is a quantitative descriptor for the concentration of missing cluster defects in the UiO-66 framework.[50]

3) The total modulator to BDC molar ratio $\left(\frac{\text{Tot. Mod.}}{\text{BDC}} m_R\right)$ is a quantitative descriptor for the concentration of monocarboxylate terminated defects in the sample.

4) The number of linker deficiencies per Zr_6 formula unit (i.e. the value of x in composition $Zr_6O_{6+x}(BDC)_{6-x}$) is an obvious descriptor for the overall defectivity of the material.
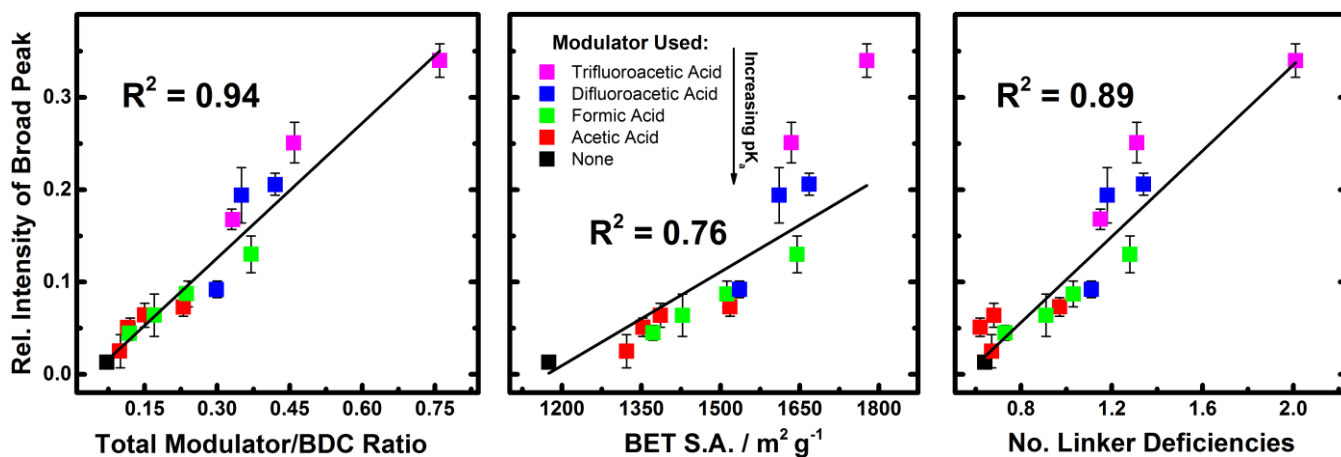
Figure 10. Graphs and linear fits obtained when the relative intensity of the broad peak ($Rel(I)_{B.P.}$) is plotted against: left plot - the total modulator to BDC ratio $\left(\frac{\text{Tot. Mod.}}{\text{BDC}} \mathbf{m_R}\right)$; middle plot – the **BET surface area**; right plot – the number of linker deficiencies per Zr_6 formula unit (i.e. the value of $\boldsymbol{x}$ in composition $\mathbf{Zr_6O_{6+x}(BDC)_{6-x}}$). Due to its aforementioned MIL-140 impurity (see Section **5.14** of SI), the data point corresponding to 6Trif has been omitted from the middle plot.

To explore the relationship between the four "defectivity descriptors", the $Rel(I)_{B.P.}$ values were plotted against the other 3 parameters, resulting in the 3 graphs presented in **Figure 10** above. For convenience, all of the data used to plot the three graphs is summarized in **Table S25**. As can be seen, the defectivity descriptors are indeed positively correlated with one another. Before delving deeper into these correlations, it is of utmost importance to emphasize that just 1 of the 4 defectivity descriptors (the relative intensity of the broad peak, $Rel(I)_{B.P.}$) is exclusively associated with only one type of defect (missing cluster defects), while the others could be influenced by the presence of *either* missing linker *or* missing cluster defects. This point is pivotal for attaining information on the nature of the defects. For example, the fact that there is a strong linear ($R^2 = 0.94$) relationship between $Rel(I)_{B.P.}$ and $\frac{\text{Tot. Mod.}}{\text{BDC}} \mathbf{m_R}$ strongly suggests that the monocarboxylate ligands are incorporated almost exclusively as compensation for missing cluster defects (refer back to **Figure 1** to visualize this scenario, where the monocarboxylate is trifluoroacetate). Likewise, the linear ($R^2 = 0.89$) relationship between $Rel(I)_{B.P.}$ and the number of linker deficiencies per Zr_6 formula unit ($\boldsymbol{x}$) implies that the linker deficiencies are almost exclusively due to missing cluster defects (recall that there are $(6 - 4) = \underline{\mathbf{2}}$ linker deficiencies per Zr_6 formula unit in the pure **reo** phase, $\mathbf{Zr_6O_6(BDC)_4(Mod)_4}$, where **Mod** is a monocarboxylate (trifluoroacetate in **Figure 1**)).

However, the relationship between $Rel(I)_{B.P.}$ and the **BET surface area** is far from linear ($R^2 = 0.76$). This can be explained by the fact that four different monocarboxylate ligands (formate, acetate, difluoroacetate, or trifluoroacetate) compensate for the missing cluster defects in the samples. These 4 ligands have significantly different molecular weights, and thus the crystallographic densities of the samples will vary considerably. Such variations in density strongly impacts the BET surface area of the material (given in meters squared per gram), an obvious point which became even more conspicuous when

analyzing our simulated N_2 adsorption isotherms (see **Section 5.4** of the SI). Thus, the **BET surface areas** of the samples do not solely depend on their defectivity, resulting in the ob-

served non-linear relationship between **BET S.A.** and $Rel(I)_{B.P.}$.

Comparison of Simulated and Experimental Nitrogen Adsorption Isotherms

In order to scrutinize the conclusion that missing cluster defects are the predominant defect in the samples, we constructed 16 hypothetical defective structural models (see **Section 4** in the SI for details) and simulated their nitrogen adsorption isotherms. Comparing the simulated isotherms with those obtained experimentally allows us to discern the type of defect which best accounts for the porosity of our samples.

The reliability of the simulations is validated by **Figure S66** in the SI, where it can be seen that the isotherm simulated from the ideal UiO-66 structural model almost exactly matches that experimentally obtained on a near defect free UiO-66 sample (and those simulated in previous studies).[33, 68] The sample, named UiO-66-Ideal (UiO-66-Ideal-Calcined in **Figure S65**), was obtained by an optimized version of the synthesis procedure we promoted in previous work[59] (see **Section 1.3** of the SI for full details of the method). Its near defect free status is evidenced by extensive characterization results presented in **Section 5.13** of the SI. We feel that UiO-66-Ideal should be considered as a "benchmark" material to which UiO-66 samples obtained by other methods should be compared.

Given the above validation, our simulated and experimental isotherms can be freely compared. The clearest example is presented in **Figure 11**, where the isotherms experimentally obtained on the difluoroacetic acid modulated samples are compared with those simulated from the difluoroacetate terminated defective structural models (see **Section 4** of the SI for details).
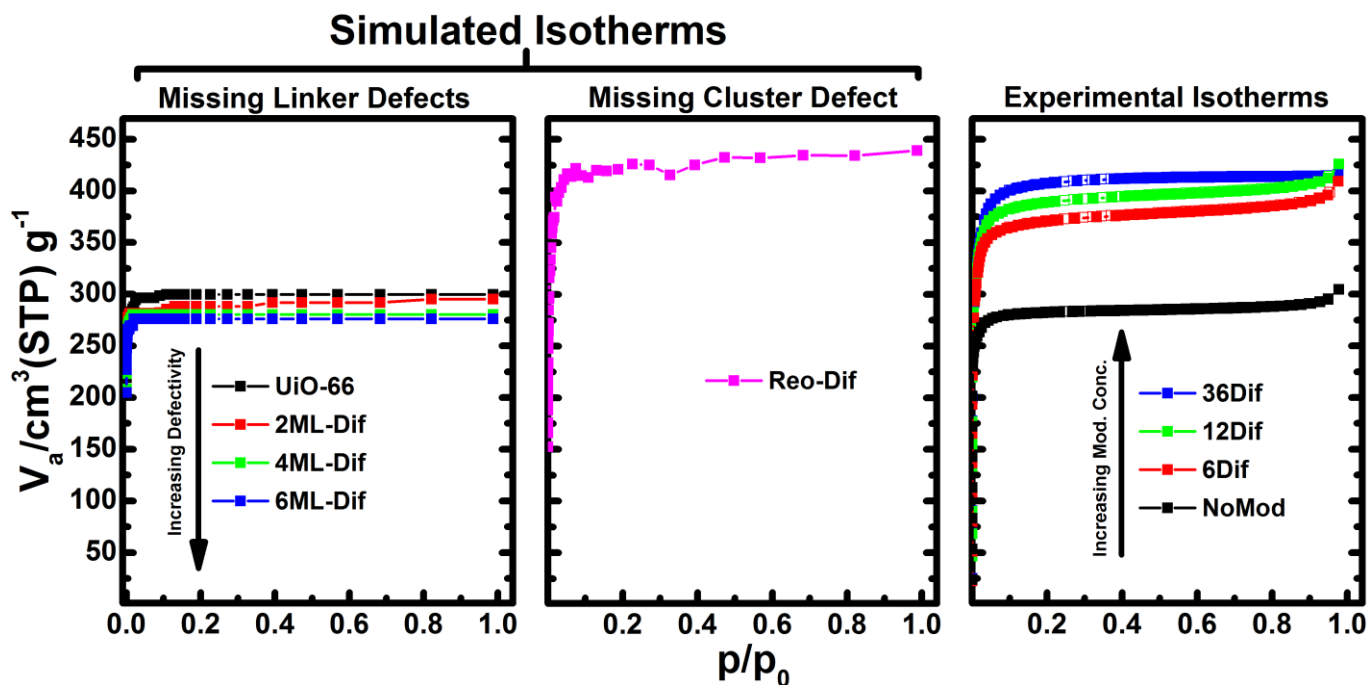
Figure 11. Comparison of the nitrogen adsorption isotherms experimentally obtained on the difluoroacetic acid modulated samples with those simulated from defective UiO-66 structural models with difluoroacetate terminal ligands (see **Section 4** of SI).

Comparing the experimental isotherms (rightmost plot) with those simulated from the missing linker structural models (leftmost plot, see **Section 4** of the SI for explanation of nomenclature), one can see that missing linker defects (compensated by difluoroacetate ligands) absolutely cannot account for the high porosity of our difluoroacetic acid modulated UiO-66 samples. Interestingly, the porosity of the hypothetical materials actually systematically *decreases* as the number of missing linker defects is increased. This surprising observation (also observed for the trifluoroacetate terminated models) is due to the increasing crystallographic density of the framework (see **Section 5.4.2** of the SI for in-depth discussion).

If we instead compare the experimental isotherms with that simulated from the missing cluster structural model (Reo-Dif, middle plot), one can clearly see that the hypothetical material is only slightly more porous than our difluoroacetic acid modulated UiO-66 samples. The implications of this observation are startling. The Reo-Dif isotherm is simulated from a pure **reo** model in which 1 out of 4 Zr_6 clusters is missing from every unit cell (the same structure as the right-most model in **Figure 1**, albeit with difluoroacetate as the defect compensating ligand). The fact that our difluoroacetic acid modulated UiO-66 samples are almost as porous as Reo-Dif therefore suggests that there is an enormous amount of missing cluster defects in the samples. This is consistent with the observation of a relatively intense "broad peak" in the PXRD patterns obtained on the difluoroacetic acid modulated UiO-66 samples (see **Figure 4** and **Figure 5**). It is therefore clear that missing cluster defects are by far the most prevalent defect in the difluoroacetic acid modulated materials. Similar conclusions were afforded by comparing the simulated and experimental isotherms related to the acetic, formic, and trifluoroacetic acid modulated UiO-66 samples (see **Section 5.5** of the SI). However, it must be said that the assignment is not as unequivocal for the acetic or for-

mic acid modulated materials, in which the defect concentrations are much lower than the difluoroacetic acid modulated UiO-66 samples discussed herein.

It is important to note that our findings oppose the most commonly held literature view on the defect chemistry of UiO-66 samples synthesized in the presence of monocarboxylic acid modulators under the most typical conditions ($ZrCl_4$ as Zr^{4+} source, 1 : 1 BDC : Zr ratio, DMF as solvent, crystallization temperature = 120 °C). There is a general agreement that the most prominent defects in such samples are missing linker defects compensated by deprotonated modulator molecules (see leftmost structure in **Figure 1**, where trifluoroacetate is the deprotonated modulator molecule).[49, 51, 53-57] However, none of the techniques most commonly used as evidence for this type of defect (TGA, dissolution/NMR, and nitrogen adsorption isotherms) can distinguish between missing linker defects and missing cluster defects terminated by monocarboxylates. The only routine method which can distinguish between the two types of defect is PXRD, and this was only discovered in mid-2014,[50] after the majority of the missing linker defect literature had already been published. We feel that it is highly likely that the PXRD "fingerprint" for missing cluster defects simply went unnoticed or was dismissed as background in earlier studies. Such a dismissal is especially tempting when it appears as a single broad peak as it does herein (refer back to **Figure 4**). Moreover, our comparison of simulated and experimental nitrogen adsorption isotherms is by far the most thorough study of this type in the UiO-66 defect literature. All things considered, we feel that the overall evidence for our conclusions is substantially stronger than earlier investigations.

Thermal Stability

In an earlier study, we found that missing cluster defects can have a severe impact on the thermal stability of UiO-66.[59] Following the discussion in the previous 2 sections, it is clear that the samples under study herein are also riddled with missing cluster defects. It was therefore of interest to investigate their thermal stability. To this end, we subjected 5 key samples

(NoMod, 36Ac, 36Form, 36Dif, and 36Trif) to 12 hours of heat treatment (in air) at 300, 350, 400, and 450 °C before measuring their PXRD patterns. The results are presented in **Figure S51** in the SI.

Surprisingly, all 5 samples completely retained their crystallinity after treatment at 350 °C, including the incredibly defective 36Trif. However, the samples differed in their ability to handle treatment at 400 °C; the most defective samples (36Dif and 36Trif) completely collapsed while the stability of the remaining materials systematically increased with decreasing defectivity (NoMod > 36Ac > 36Form). Missing cluster defects therefore do appear to negatively affect the stability of the material. However, the range of thermal stabilities of the samples herein is far narrower than those in our previous study, many of which partially collapsed after treatment at just 250 °C.[58] The poor stability of said samples was attributed to the presence of missing cluster defects. Given that missing clusters are also the predominant defect in the samples herein, it is somewhat surprising that there is such a discrepancy between the thermal stabilities of the two sets of samples. Nevertheless, we can think of two possible reasons for this:

1) The samples in the previous study contain larger domains of missing cluster defects. This is evidenced by the breadth of the forbidden reflections,[50] which were much narrower (and clearly resolved from one another) in the PXRD patterns obtained in our previous work.[71] It is reasonable to suggest that larger domains of missing cluster defects would be detrimental to the stability of the UiO-66 framework.

2) The identity of the defect compensating ligands. Chloride was thought to fulfil this role in the previous study,[37] while monocarboxylates are the defect terminating ligands herein. Compensation with monocarboxylates allows the clusters to retain the familiar $Zr_6O_4(OH)_4(CO_2)_{12}$ arrangement, which we imagine to be a more robust chemical environment than clusters partially terminated with Cl^- ligands.

DISCUSSION OF OVERALL FINDINGS

Combining all results presented herein, the foremost conclusions of this study are:

1) Missing cluster defects are the predominant defect in UiO-66 samples synthesized in the presence of monocarboxylic acid modulators under the most typical conditions.

2) The defects are compensated by a combination of deprotonated modulator molecules and formate (originating from the *in situ* decomposition of DMF during the MOF synthesis).

3) The concentration of missing cluster defects in the UiO-66 framework systematically increases as increasing amounts of modulator are added to the synthesis mixture.

4) The concentration of missing cluster defects in the UiO-66 framework systematically increases as the acidity of the modulator is increased.

In order to understand the origin of these conclusions, one needs to understand the chemistry occurring in the MOF syn-

thesis solution. To this end, we hypothesize that the modulator and linker compete with one another for carboxylate (CO_2^-) sites in the $Zr_6(OH)_4O_4(CO_2)_{12}$ clusters. The acids must be deprotonated before they can coordinate in this manner. To form a missing cluster defect, the deprotonated modulator needs to bind to *at least* 1 of the 12 sites on 12 different clusters, each in close proximity to one another. The geometry of these 12 clusters must be correlated such that the 12 monocarboxylates point towards the cavity where a cluster would ordinarily be found. This interpretation accounts for the first 2 conclusions above. Furthermore, it is easy to see how conclusion 3 would follow: higher concentration of modulator = more modulator ligands for the linker to compete with = increased probability of modulator remaining bound to the cluster in the product = more missing cluster defects.

Before proceeding with our discussion of the 4th conclusion, it is important to declare that the literature pK_a values presented herein were measured in aqueous conditions, and under normal circumstances one should be wary of discussing such values in the context of MOF syntheses in DMF solutions. Nevertheless, the observed trends with modulator acidity are unequivocal and it is difficult to imagine that they could appear by mere coincidence.

With this in mind, our working explanation for the 4th conclusion stems from the fact that the modulator must be deprotonated in order to coordinate to the clusters. We then apply the following logic: more acidic modulator = higher concentration of deprotonated modulator in solution = more monocarboxylate ligands for the linker to compete with = increased probability of modulator remaining bound to cluster in product = more missing cluster defects. An alternative explanation can be reached if one assumes that the strength of a Zr^{4+}-^-O_2C bond systematically increases as the pK_a of the carboxylate (in its acidic form) decreases. Indeed, Bennett and co-workers have previously claimed that the bond between trifluoroacetate and the Zr_6 cluster is particularly strong, and attributed this to the high acidity of trifluoroacetic acid.[54] However, this contradicts the generally accepted idea that the strength of a metal-ligand bond increases as the basicity of the ligand increases.[84, 85] If we instead assume that our working hypothesis is true, it is interesting to imagine the dynamics of the competition between the modulator and linker and speculate on their effects in a case by case manner:

- The pK_a's of difluoroacetic (1.24) and trifluoroacetic acid (0.23) are much lower than those of H_2BDC ($pK_{a1} = 3.51$, $pK_{a2} = 4.82$). Thus, when difluoroacetic or trifluoroacetic acid is used as a modulator, the synthesis solution is expected to contain many more deprotonated modulator molecules than deprotonated linker molecules. The modulator would therefore dominate the competition for carboxylate sites on the $Zr_6(OH)_4O_4(CO_2)_{12}$ clusters, resulting in samples with a very high concentration of missing cluster defects.

- The pK_a of formic acid (3.77) is similar to the first pK_a of the H_2BDC linker (3.51). The competition between formate and the singly deprotonated linker ($HBDC^-$) is thus expected to be fairly close. We speculate that such close competition allows formic acid to behave more like a modulator in the traditional sense,[43, 86, 87] where ligand (carboxylate) exchange reactions between formate and $HBDC^-$ are favored, inhibiting crystal nucleation and promoting growth. This is

consistent with the formation of relatively large octahedral crystals when formic acid is used as a modulator (SEM images are presented in **Figure S52**, see the SI). However, formic acid is considerably more acidic than the singly deprotonated linker (HBDC$^-$, pK$_a$ = 4.82). The synthesis solution is therefore expected to contain many more deprotonated modulator molecules (formate) than doubly deprotonated linker molecules (BDC^{2-}). As a result, formate would still "win" many of the carboxylate sites on the **Zr$_6$(OH)$_4$O$_4$(CO$_2$)$_{12}$** clusters, resulting in the observation of a moderate amount of missing cluster defects when formic acid is used as a modulator.

- The pK$_a$ of acetic acid (4.76) is very similar to the second pK$_a$ of the H$_2$BDC linker (4.82). The competition between acetate and the doubly deprotonated linker (BDC^{2-}) is therefore expected to be very close. Following the same logic as in the previous bullet point, this close competition inhibits crystal nucleation and promotes growth, resulting in the formation of large octahedral crystals when acetic acid is used as a modulator (SEM images are presented in **Figure S52** in the SI). Furthermore, the meagre acidity of acetic acid ensures that the concentration of acetate in the synthesis solution would be rather low. Thus, only a small amount of acetate is expected to become incorporated into the material, resulting in the observation of a low concentration of missing cluster defects when acetic acid is used as a modulator.

POTENTIAL FOR SCOPE

The discussion outlined in the previous section shows that our results can be fully explained if we assume that our hypothesis based on the competition between the modulator and linker is true. This paper concerns only UiO-66, but we believe that our hypothesis may be applicable to "Zr$_6$ MOFs" in general. If so, this work could greatly aid MOF chemists to make informed choices when selecting a modulator for their syntheses. For example, a general strategy for the synthesis of large crystals of relatively low defectivity could be to make the competition between the modulator and the linker as close as possible. According to our hypothesis, this can be achieved by using a monocarboxylic acid modulator whose pK$_a$ is similar to that of the second linker deprotonation (the equivalent of using acetic acid in the synthesis of UiO-66). If one instead wishes to purposely synthesize a highly defective (and thus, more porous) material, then it is best to select a modulator which dominates its competition with the linker. According to our hypothesis, this can be achieved by using a monocarboxylic acid modulator whose Pk$_a$ is much lower than those of the linker. This may be difficult to achieve if the linker is highly acidic, but in most cases trifluoroacetic acid (the most acidic carboxylic acid in common use) would be an excellent choice of modulator.

When further considering the scope of this work, we feel it is important to declare that our hypothesis surely has its limits. All of the modulators investigated herein are liquids with complete miscibility in DMF, meaning that solubility effects could be completely disregarded. This allowed us to confidently study the influence of modulator acidity in isolation. However, it is reasonable to suggest that solubility and/or steric effects will likely have a significant impact on the defect chemistry of UiO-66 samples synthesized in the presence of solid modulators e.g. benzoic acid. Such samples may not fit into the strikingly systematic acidity trends observed herein.

CONCLUSION

We have performed a deep investigation into the defect chemistry of UiO-66 samples synthesized in the presence of monocarboxylic acid modulators under the most typical conditions (ZrCl$_4$ as Zr^{4+} source, BDC : Zr ratio = 1 : 1, DMF as solvent, crystallization temperature = 120 °C). The concentration and acidity (pK$_a$) of the modulator was systematically varied in a total of 15 UiO-66 syntheses.

Qualitative and quantitative analysis of our multi-technique characterization data revealed that the defectivity of UiO-66 can be systematically tuned to a remarkable extent, resulting in a series of samples with a wide range of porosities and compositions. Specifically, the defectivity of the material was found to systematically and dramatically increase as the concentration and/or acidity of the modulator was increased. Our dissolution/NMR results showed that the defect compensating ligands are a combination of deprotonated modulator molecules and formate (originating from the *in situ* decomposition of DMF during the MOF synthesis).

Four quantitative "defectivity descriptors" were derived from PXRD, nitrogen adsorption, dissolution/NMR, and TGA data. Analysis of the correlations between these descriptors afforded the conclusion that missing clusters are the predominant defect in the samples. This conclusion was strongly supported by simulated nitrogen adsorption isotherms.

To account for these observations, we speculated on the chemistry occurring in the UiO-66 synthesis solution, and formulated a simple hypothesis based on the competition between the linker and modulator (see section headed "Discussion of overall findings"). We believe that our hypothesis could be applicable to the synthesis of "Zr$_6$ MOFs" in general; allowing MOF chemists to make an informed decision when deliberating which modulator to use in their syntheses (see section headed "Potential for scope" for more on this).

AUTHOR INFORMATION

Corresponding Author

* k.p.lillerud@kjemi.uio.no

ACKNOWLEDGMENT

ASSOCIATED CONTENT

Supporting Information

Details of synthesis, characterization, and quantitative analysis methods, description of defective structural models, discussion of PXRD, dissolution/NMR, TGA-DSC, ATR-IR, EDX, SEM, thermal stability tests, density measurements, and N$_2$ sorption (both simulated and experimental) results. This material is available free of charge at http://pubs.acs.org.

REFERENCES

(1) Mondloch, J.; Katz, M.; Planas, N.; Semrouni, D.; Gagliardi, L.; Hupp, J.; Farha, O., Are Zr-6-based MOFs water stable? Linker hydrolysis

vs. capillary-force-driven channel collapse. *Chem. Commun.* **2014,** 50, 8944-8946.

(2) Kalidindi, S.; Nayak, S.; Briggs, M.; Jansat, S.; Katsoulidis, A.; Miller, G.; Warren, J.; Antypov, D.; Cora, F.; Slater, B.; Prestly, M.; Marti-Gastaldo, C.; Rosseinsky, M., Chemical and Structural Stability of Zirconium-based Metal-Organic Frameworks with Large Three-Dimensional Pores by Linker Engineering. *Angew. Chem. Int. Edit.* **2015,** 54, 221-226.

(3) Feng, D.; Chung, W.; Wei, Z.; Gu, Z.; Jiang, H.; Chen, Y.; Darensbourg, D.; Zhou, H., Construction of Ultrastable Porphyrin Zr Metal-Organic Frameworks through Linker Elimination. *J. Am. Chem. Soc.* **2013,** 135, 17105-17110.

(4) Jiang, H.; Feng, D.; Wang, K.; Gu, Z.; Wei, Z.; Chen, Y.; Zhou, H., An Exceptionally Stable, Porphyrinic Zr Metal-Organic Framework Exhibiting pH-Dependent Fluorescence. *J. Am. Chem. Soc.* **2013,** 135, 13934-13938.

(5) Reinsch, H.; Stassen, I.; Bueken, B.; Lieb, A.; Ameloot, R.; De Vos, D., First examples of aliphatic zirconium MOFs and the influence of inorganic anions on their crystal structures. *Crystengcomm* **2015,** 17, 331-337.

(6) Reinsch, H.; Bueken, B.; Vermoortele, F.; Stassen, I.; Lieb, A.; Lillerud, K.; De Vos, D., Green synthesis of zirconium-MOFs. *Crystengcomm* **2015,** 17, 4070-4074.

(7) Feng, D.; Gu, Z.; Chen, Y.; Park, J.; Wei, Z.; Sun, Y.; Bosch, M.; Yuan, S.; Zhou, H., A Highly Stable Porphyrinic Zirconium Metal-Organic Framework with shp-a Topology. *J. Am. Chem. Soc.* **2014,** 136, 17714-17717.

(8) Feng, D.; Wang, K.; Su, J.; Liu, T.; Park, J.; Wei, Z.; Bosch, M.; Yakovenko, A.; Zou, X.; Zhou, H., A Highly Stable Zeotype Mesoporous Zirconium Metal-Organic Framework with Ultralarge Pores. *Angew. Chem. Int. Edit.* **2015,** 54, 149-154.

(9) Cavka, J.; Jakobsen, S.; Olsbye, U.; Guillou, N.; Lamberti, C.; Bordiga, S.; Lillerud, K., A new zirconium inorganic building brick forming metal organic frameworks with exceptional stability. *J. Am. Chem. Soc.* **2008,** 130, 13850-13851.

(10) Schaate, A.; Roy, P.; Preusse, T.; Lohmeier, S.; Godt, A.; Behrens, P., Porous Interpenetrated Zirconium-Organic Frameworks (PIZOFs): A Chemically Versatile Family of Metal-Organic Frameworks. *Chem. Eur. J.* **2011,** 17, 9320-9325.

(11) Wang, R.; Wang, Z.; Xu, Y.; Dai, F.; Zhang, L.; Sun, D., Porous Zirconium Metal-Organic Framework Constructed from 2D -> 3D Interpenetration Based on a 3,6-Connected kgd Net. *Inorg. Chem.* **2014,** 53, 7086-7088.

(12) Ma, J.; Wong-Foy, A.; Matzger, A., The Role of Modulators in Controlling Layer Spacings in a Tritopic Linker Based Zirconium 2D Microporous Coordination Polymer. *Inorg. Chem.* **2015,** 54, 4591-4593.

(13) Yuan, S.; Lu, W.; Chen, Y.; Zhang, Q.; Liu, T.; Feng, D.; Wang, X.; Qin, J.; Zhou, H., Sequential Linker Installation: Precise Placement of Functional Groups in Multivariate Metal-Organic Frameworks. *J. Am. Chem. Soc.* **2015,** 137, 3177-3180.

(14) Zhang, M.; Chen, Y.; Bosch, M.; Gentle, T.; Wang, K.; Feng, D.; Wang, Z.; Zhou, H., Symmetry-Guided Synthesis of Highly Porous Metal-Organic Frameworks with Fluorite Topology. *Angew. Chem. Int. Edit.* **2014,** 53, 815-818.

(15) Morris, W.; Volosskiy, B.; Demir, S.; Gandara, F.; McGrier, P.; Furukawa, H.; Cascio, D.; Stoddart, J.; Yaghi, O., Synthesis, Structure, and Metalation of Two New Highly Porous Zirconium Metal-Organic Frameworks. *Inorg. Chem.* **2012,** 51, 6443-6445.

(16) Bon, V.; Senkovska, I.; Weiss, M.; Kaskel, S., Tailoring of network dimensionality and porosity adjustment in Zr- and Hf-based MOFs. *Crystengcomm* **2013,** 15, 9572-9577.

(17) Liu, T.; Feng, D.; Chen, Y.; Zou, L.; Bosch, M.; Yuan, S.; Wei, Z.; Fordham, S.; Wang, K.; Zhou, H., Topology-Guided Design and Syntheses of Highly Stable Mesoporous Porphyrinic Zirconium Metal-Organic Frameworks with High Surface Area. *J. Am. Chem. Soc.* **2015,** 137, 413-419.

(18) Liang, W.; Chevreau, H.; Ragon, F.; Southon, P.; Peterson, V.; D'Alessandro, D., Tuning pore size in a zirconium-tricarboxylate metal-organic framework. *Crystengcomm* **2014,** 16, 6530-6533.

(19) Wang, T.; Bury, W.; Gomez-Gualdron, D.; Vermeulen, N.; Mondloch, J.; Deria, P.; Zhang, K.; Moghadam, P.; Sarjeant, A.; Snurr, R.; Stoddart, J.; Hupp, J.; Farha, O., Ultrahigh Surface Area Zirconium MOFs and Insights into the Applicability of the BET Theory. *J. Am. Chem. Soc.* **2015,** 137, 3585-3591.

(20) Deria, P.; Gomez-Gualdron, D.; Bury, W.; Schaef, H.; Wang, T.; Thallapally, P.; Sarjeant, A.; Snurr, R.; Hupp, J.; Farha, O., Ultraporous, Water Stable, and Breathing Zirconium-Based Metal-Organic Frameworks with ftw Topology. *J. Am. Chem. Soc.* **2015,** 137, 13183-13190.

(21) Mondloch, J.; Bury, W.; Fairen-Jimenez, D.; Kwon, S.; DeMarco, E.; Weston, M.; Sarjeant, A.; Nguyen, S.; Stair, P.; Snurr, R.; Farha, O.; Hupp, J., Vapor-Phase Metalation by Atomic Layer Deposition in a Metal-Organic Framework. *J. Am. Chem. Soc.* **2013,** 135, 10294-10297.

(22) Furukawa, H.; Gandara, F.; Zhang, Y.; Jiang, J.; Queen, W.; Hudson, M.; Yaghi, O., Water Adsorption in Porous Metal-Organic Frameworks and Related Materials. *J. Am. Chem. Soc.* **2014,** 136, 4369-4381.

(23) Gutov, O.; Bury, W.; Gomez-Gualdron, D.; Krungleviciute, V.; Fairen-Jimenez, D.; Mondloch, J.; Sarjeant, A.; Al-Juaid, S.; Snurr, R.; Hupp, J.; Yildirim, T.; Farha, O., Water-Stable Zirconium-Based Metal-Organic Framework Material with High-Surface Area and Gas-Storage Capacities. *Chem. Eur. J* **2014,** 20, 12389-12393.

(24) Bueken, B.; Reinsch, H.; Reimer, N.; Stassen, I.; Vermoortele, F.; Ameloot, R.; Stock, N.; Kirschhock, C.; De Vos, D., A zirconium squarate metal-organic framework with modulator-dependent molecular sieving properties. *Chem. Commun.* **2014,** 50, 10055-10058.

(25) Feng, D.; Gu, Z.; Li, J.; Jiang, H.; Wei, Z.; Zhou, H., Zirconium-Metalloporphyrin PCN-222: Mesoporous Metal-Organic Frameworks with Ultrahigh Stability as Biomimetic Catalysts. *Angew. Chem. Int. Edit.* **2012,** 51, 10307-10310.

(26) Bon, V.; Senkovska, I.; Baburin, I.; Kaskel, S., Zr- and Hf-Based Metal-Organic Frameworks: Tracking Down the Polymorphism. *Cryst. Growth Des.* **2013,** 13, 1231-1237.

(27) Bon, V.; Senkovskyy, V.; Senkovska, I.; Kaskel, S., Zr(IV) and Hf(IV) based metal-organic frameworks with reo-topology. *Chem. Commun.* **2012,** 48, 8407-8409.

(28) Hu, Z.; Faucher, S.; Zhuo, Y.; Sun, Y.; Wang, S.; Zhao, D., Combination of Optimization and Metalated-Ligand Exchange: An Effective Approach to Functionalize UiO-66(Zr) MOFs for CO2 Separation. *Chem. Eur. J.* **2015,** 21, 17246-17255.

(29) Yee, K.; Reimer, N.; Liu, J.; Cheng, S.; Yiu, S.; Weber, J.; Stock, N.; Xu, Z., Effective Mercury Sorption by Thiol-Laced Metal-Organic Frameworks: in Strong Acid and the Vapor Phase. *J. Am. Chem. Soc.* **2013,** 135, 7795-7798.

(30) Pullen, S.; Fei, H.; Orthaber, A.; Cohen, S.; Ott, S., Enhanced Photochemical Hydrogen Production by a Molecular Diiron Catalyst Incorporated into a Metal-Organic Framework. *J. Am. Chem. Soc.* **2013,** 135, 16997-17003.

(31) Biswas, S.; Zhang, J.; Li, Z.; Liu, Y.; Grzywa, M.; Sun, L.; Volkmer, D.; Van der Voort, P., Enhanced selectivity of CO2 over CH4 in sulphonate-, carboxylate- and iodo-functionalized UiO-66 frameworks. *Dalton Trans.* **2013,** 42, 4730-4737.

(32) Huang, Y.; Qin, W.; Li, Z.; Li, Y., Enhanced stability and CO2 affinity of a UiO-66 type metal-organic framework decorated with dimethyl groups. *Dalton Trans.* **2012,** 41, 9283-9285.

(33) Katz, M.; Brown, Z.; Colon, Y.; Siu, P.; Scheidt, K.; Snurr, R.; Hupp, J.; Farha, O., A facile synthesis of UiO-66, UiO-67 and their derivatives. *Chem. Commun.* **2013,** 49, 9449-9451.

(34) Biswas, S.; Van der Voort, P., A General Strategy for the Synthesis of Functionalised UiO-66 Frameworks: Characterisation, Stability and CO2 Adsorption Properties. *Eur. J. Inorg. Chem.* **2013,** 2154-2160.

(35) Garibay, S.; Cohen, S., Isoreticular synthesis and modification of frameworks with the UiO-66 topology. *Chem. Commun.* **2010,** 46, 7700-7702.

(36) Foo, M.; Horike, S.; Fukushima, T.; Hijikata, Y.; Kubota, Y.; Takata, M.; Kitagawa, S., Ligand-based solid solution approach to stabilisation of sulphonic acid groups in porous coordination polymer Zr6O4(OH)(4)(BDC)(6) (UiO-66). *Dalton Trans.* **2012,** 41, 13791-13794.

(37) Fei, H.; Cohen, S., Metalation of a Thiocatechol-Functionalized Zr(IV)-Based Metal-Organic Framework for Selective C-H Functionalization. *J. Am. Chem. Soc.* **2015,** 137, 2191-2194.

(38) Jasuja, H.; Zang, J.; Sholl, D.; Walton, K., Rational Tuning of Water Vapor and CO2 Adsorption in Highly Stable Zr-Based MOFs. *J. Phys. Chem. C* **2012,** 116, 23526-23532.

(39) Fei, H.; Shin, J.; Meng, Y.; Adelhardt, M.; Sutter, J.; Meyer, K.; Cohen, S., Reusable Oxidation Catalysis Using Metal-Monocatecholato Species in a Robust Metal-Organic Framework. *J. Am. Chem. Soc.* **2014,** 136, 4965-4973.

(40) Kandiah, M.; Nilsen, M.; Usseglio, S.; Jakobsen, S.; Olsbye, U.; Tilset, M.; Larabi, C.; Quadrelli, E.; Bonino, F.; Lillerud, K., Synthesis and Stability of Tagged UiO-66 Zr-MOFs. *Chem. Mater.* **2010,** 22, 6632-6640.

(41) Nickerl, G.; Senkovska, I.; Kaskel, S., Tetrazine functionalized zirconium MOF as an optical sensor for oxidizing gases. *Chem. Commun.* **2015,** 51, 2280-2282.

(42) Yang, Q.; Vaesen, S.; Ragon, F.; Wiersum, A.; Wu, D.; Lago, A.; Devic, T.; Martineau, C.; Taulelle, F.; Llewellyn, P.; Jobic, H.; Zhong, C.; Serre, C.; De Weireld, G.; Maurin, G., A Water Stable Metal-Organic Framework with Optimal Features for CO2 Capture. *Angew. Chem. Int. Edit.* **2013,** 52, 10316-10320.

(43) Schaate, A.; Roy, P.; Godt, A.; Lippke, J.; Waltz, F.; Wiebcke, M.; Behrens, P., Modulated Synthesis of Zr-Based Metal-Organic Frameworks: From Nano to Single Crystals. *Chem. Eur. J.* **2011,** 17, 6643-6651.

(44) Tulig, K.; Walton, K., An alternative UiO-66 synthesis for HCl-sensitive nanoparticle encapsulation. *RSC Adv.* **2014,** 4, 51080-51083.

(45) Taddei, M.; Dau, P.; Cohen, S.; Ranocchiari, M.; van Bokhoven, J.; Costantino, F.; Sabatini, S.; Vivani, R., Efficient microwave assisted synthesis of metal-organic framework UiO-66: optimization and scale up. *Dalton Trans.* **2015,** 44, 14019-14026.

(46) Li, Y.; Liu, Y.; Gao, W.; Zhang, L.; Liu, W.; Lu, J.; Wang, Z.; Deng, Y., Microwave-assisted synthesis of UIO-66 and its adsorption performance towards dyes. *Crystengcomm* **2014,** 16, 7037-7042.

(47) Ren, J.; Langmi, H.; North, B.; Mathe, M.; Bessarabov, D., Modulated synthesis of zirconium-metal organic framework (Zr-MOF) for hydrogen storage applications. *Int. J. Hydrogen Energy* **2014,** 39, 890-895.

(48) Anjum, M. W.; Vermoortele, F.; Khan, A. L.; Bueken, B.; De Vos, D. E.; Vankelecom, I. F. J., Modulated UiO-66-Based Mixed-Matrix Membranes for CO2 Separation. *ACS Appl. Mater. Interfaces* **2015,** 7, 25193-25201.

(49) Vandichel, M.; Hajek, J.; Vermoortele, F.; Waroquier, M.; De Vos, D.; Van Speybroeck, V., Active site engineering in UiO-66 type metal-organic frameworks by intentional creation of defects: a theoretical rationalization. *Crystengcomm* **2015,** 17, 395-406.

(50) Cliffe, M.; Wan, W.; Zou, X.; Chater, P.; Kleppe, A.; Tucker, M.; Wilhelm, H.; Funnell, N.; Coudert, F.; Goodwin, A., Correlated defect nanoregions in a metal-organic framework. *Nat. Commun.* **2014,** 5.

(51) Taylor, J.; Dekura, S.; Ikeda, R.; Kitagawa, H., Defect Control To Enhance Proton Conductivity in a Metal-Organic Framework. *Chem. Mater.* **2015,** 27, 2286-2289.

(52) Cliffe, M.; Hill, J.; Murray, C.; Coudert, F.; Goodwin, A., Defect-dependent colossal negative thermal expansion in UiO-66(Hf) metal-organic framework. *Phys. Chem. Chem. Phys.* **2015,** 17, 11586-11592.

(53) Xydias, P.; Spanopoulos, I.; Klontzas, E.; Froudakis, G. E.; Trikalitis, P. N., Drastic enhancement of the CO2 adsorption properties in sulfone-functionalized Zr- and Hf-UiO-67 MOFs with hierarchical mesopores. *Inorg. Chem.* **2014,** 53, 679-81.

(54) Van de Voorde, B.; Stassen, I.; Bueken, B.; Vermoortele, F.; De Vos, D.; Ameloot, R.; Tan, J.; Bennett, T., Improving the mechanical stability of zirconium-based metal-organic frameworks by incorporation of acidic modulators. *J. Mater. Chem. A* **2015,** 3, 1737-1742.

(55) Gutov, O.; Hevia, M.; Escudero-Adan, E.; Shafir, A., Metal-Organic Framework (MOF) Defects under Control: Insights into the Missing Linker Sites and Their Implication in the Reactivity of Zirconium-Based Frameworks. *Inorg. Chem.* **2015,** 54, 8396-8400.

(56) Vermoortele, F.; Bueken, B.; Le Bars, G.; Van de Voorde, B.; Vandichel, M.; Houthoofd, K.; Vimont, A.; Daturi, M.; Waroquier, M.; Van Speybroeck, V.; Kirschhock, C.; De Vos, D., Synthesis Modulation as a Tool To Increase the Catalytic Activity of Metal-Organic Frameworks: The Unique Case of UiO-66(Zr). *J. Am. Chem. Soc.* **2013,** 135, 11465-11468.

(57) Ren, J.; Langmi, H. W.; Musyoka, N. M.; Mathe, M.; Kang, X.; Liao, S., Tuning Defects to Facilitate Hydrogen Storage in Core-shell MIL-101(Cr)@UiO-66(Zr) Nanocrystals. *Mater. Today: Proc.* **2015,** 2, 3964-3972.

(58) Wu, H.; Chua, Y.; Krungleviciute, V.; Tyagi, M.; Chen, P.; Yildirim, T.; Zhou, W., Unusual and Highly Tunable Missing-Linker Defects in Zirconium Metal-Organic Framework UiO-66 and Their Important Effects on Gas Adsorption. *J. Am. Chem. Soc.* **2013,** 135, 10525-10532.

(59) Shearer, G. C.; Chavan, S.; Ethiraj, J.; Vitillo, J. G.; Svelle, S.; Olsbye, U.; Lamberti, C.; Bordiga, S.; Lillerud, K. P., Tuned to Perfection: Ironing Out the Defects in Metal–Organic Framework UiO-66. *Chem. Mater.* **2014,** 26, 4068-4071.

(60) Piscopo, C.; Polyzoidis, A.; Schwarzer, M.; Loebbecke, S., Stability of UiO-66 under acidic treatment: Opportunities and limitations for post-synthetic modifications. *Microporous Mesoporous Mater.* **2015,** 208, 30-35.

(61) Bristow, J. K.; Svane, K. L.; Tiana, D.; Skelton, J. M.; Gale, J. D.; Walsh, A., Free Energy of Ligand Removal in the Metal–Organic Framework UiO-66. *The Journal of Physical Chemistry C* **2016**.

(62) Thornton, A. W.; Babarao, R.; Jain, A.; Trousselet, F.; Coudert, F. X., Defects in metal-organic frameworks: a compromise between adsorption and stability? *Dalton Transactions* **2016,** 45, 4352-4359.

(63) Vermoortele, F.; Vandichel, M.; Van de Voorde, B.; Ameloot, R.; Waroquier, M.; Van Speybroeck, V.; De Vos, D., Electronic Effects of Linker Substitution on Lewis Acid Catalysis with Metal-Organic Frameworks. *Angew. Chem. Int. Edit.* **2012,** 51, 4887-4890.

(64) Katz, M.; Klet, R.; Moon, S.; Mondloch, J.; Hupp, J.; Farha, O., One Step Backward Is Two Steps Forward: Enhancing the Hydrolysis Rate of UiO-66 by Decreasing [OH-]. *ACS Catal.* **2015,** 5, 4637-4642.

(65) Canivet, J.; Vandichel, M.; Farrusseng, D., Origin of highly active metal-organic framework catalysts: defects? Defects! *Dalton Trans.* **2016**.

(66) Yang, D.; Odoh, S. O.; Borycz, J.; Wang, T. C.; Farha, O. K.; Hupp, J. T.; Cramer, C. J.; Gagliardi, L.; Gates, B. C., Tuning Zr-6 Metal-Organic Framework (MOF) Nodes as Catalyst Supports: Site Densities and Electron-Donor Properties Influence Molecular Iridium Complexes as Ethylene Conversion Catalysts. *Acs Catalysis* **2016,** 6, 235-247.

(67) Nasalevich, M. A.; Hendon, C. H.; Santaclara, J. G.; Svane, K.; van der Linden, B.; Veber, S. L.; Fedin, M. V.; Houtepen, A. J.; van der Veen, M. A.; Walsh, A.; Gascon, J., Electronic origins of photocatalytic activity in d(0) metal organic frameworks. *Scientific Reports* **2016,** 6.

(68) Ghosh, P.; Colon, Y.; Snurr, R., Water adsorption in UiO-66: the importance of defects. *Chem. Commun.* **2014,** 50, 11329-11331.

(69) Liang, W.; Coghlan, C. J.; Ragon, F.; Rubio-Martinez, M.; D'Alessandro, D. M.; Babarao, R., Defect engineering of UiO-66 for CO2 and H2O uptake - a combined experimental and simulation study. *Dalton Transactions* **2016,** 45, 4496-4500.

(70) Li, B.; Zhu, X.; Hu, K.; Li, Y.; Feng, J.; Shi, J.; Gu, J., Defect creation in metal-organic frameworks for rapid and controllable decontamination of roxarsone from aqueous solution. *J. Hazard. Mater.* **2016,** 302, 57-64.

(71) Howarth, A.; Liu, Y.; Hupp, J.; Farha, O., Metal-organic frameworks for applications in remediation of oxyanion/cation-contaminated water. *Crystengcomm* **2015,** 17, 7245-7253.

(72) DeCoste, J. B.; Demasky, T. J.; Katz, M. J.; Farha, O. K.; Hupp, J. T., A UiO-66 analogue with uncoordinated carboxylic acids for the broad-spectrum removal of toxic chemicals. *New J. Chem.* **2015,** 39, 2396-2399.

(73) Trickett, C.; Gagnon, K.; Lee, S.; Gandara, F.; Burgi, H.; Yaghi, O., Definitive Molecular Level Characterization of Defects in UiO-66 Crystals. *Angew. Chem. Int. Edit.* **2015,** 54, 11162-11167.

(74) Øien, S.; Wragg, D.; Reinsch, H.; Svelle, S.; Bordiga, S.; Lamberti, C.; Lillerud, K., Detailed Structure Analysis of Atomic Positions and Defects in Zirconium Metal-Organic Frameworks. *Cryst. Growth Des.* **2014,** 14, 5370-5372.

(75) Valenzano, L.; Civalleri, B.; Chavan, S.; Bordiga, S.; Nilsen, M.; Jakobsen, S.; Lillerud, K.; Lamberti, C., Disclosing the Complex Structure of UiO-66 Metal Organic Framework: A Synergic Combination of Experiment and Theory. *Chem. Mater.* **2011,** 23, 1700-1718.

(76) Han, Y.; Liu, M.; Li, K.; Zuo, Y.; Wei, Y.; Xu, S.; Zhang, G.; Song, C.; Zhang, Z.; Guo, X., Facile synthesis of morphology and size-controlled zirconium metal-organic framework UiO-66: the role of hydrofluoric acid in crystallization. *Crystengcomm* **2015,** 17, 6434-6440.

(77) Waitschat, S.; Wharmby, M.; Stock, N., Flow-synthesis of carboxylate and phosphonate based metal-organic frameworks under non-solvothermal reaction conditions. *Dalton Trans.* **2015,** 44, 11235-11240.

(78) Nouar, F.; Breeze, M.; Campo, B.; Vimont, A.; Clet, G.; Daturi, M.; Devic, T.; Walton, R.; Serre, C., Tuning the properties of the UiO-66 metal organic framework by Ce substitution. *Chem. Commun.* **2015,** 51, 14458-14461.

(79) Wang, K.; Li, C.; Liang, Y.; Han, T.; Huang, H.; Yang, Q.; Liu, D.; Zhong, C., Rational construction of defects in a metal-organic framework for highly efficient adsorption and separation of dyes. *Chem. Eng. J.* **2016,** 289, 486-493.

(80) Shearer, G.; Forselv, S.; Chavan, S.; Bordiga, S.; Mathisen, K.; Bjørgen, M.; Svelle, S.; Lillerud, K., In Situ Infrared Spectroscopic and Gravimetric Characterisation of the Solvent Removal and Dehydroxylation of the Metal Organic Frameworks UiO-66 and UiO-67. *Top. Catal.* **2013,** 56, 770-782.

(81) Lawrence, M. C.; Schneider, C.; Katz, M. J., Determining the structural stability of UiO-67 with respect to time: a solid-state NMR investigation. *Chem. Commun.* **2016,** 52, 4971-4974.

(82) Ling, S.; Slater, B., Dynamic acidity in defective UiO-66. *Chemical Science* **2016**.

(83) Wiersum, A.; Soubeyrand-Lenoir, E.; Yang, Q.; Moulin, B.; Guillerm, V.; Ben Yahia, M.; Bourrelly, S.; Vimont, A.; Miller, S.; Vagner, C.; Daturi, M.; Clet, G.; Serre, C.; Maurin, G.; Llewellyn, P., An Evaluation of UiO-66 for Gas-Based Applications. *Chem. Asian J.* **2011,** 6, 3270-3280.

(84) Colombo, V.; Galli, S.; Choi, H.; Han, G.; Maspero, A.; Palmisano, G.; Masciocchi, N.; Long, J., High thermal and chemical stability in pyrazolate-bridged metal-organic frameworks with exposed metal sites. *Chem. Sci.* **2011,** 2, 1311-1319.

(85) Nimmermark, A.; Ohrstrom, L.; Reedijk, J., Metal-ligand bond lengths and strengths: are they correlated? A detailed CSD analysis. *Z. Kristallogr.* **2013,** 228, 311-317.

(86) Bosch, M.; Zhang, M.; Zhou, H.-C., Increasing the Stability of Metal-Organic Frameworks. *Adv. Chem.* **2014,** 2014, 8.

(87) Feng, D.; Wang, K.; Wei, Z.; Chen, Y.; Simon, C.; Arvapally, R.; Martin, R.; Bosch, M.; Liu, T.; Fordham, S.; Yuan, D.; Omary, M.; Haranczyk, M.; Smit, B.; Zhou, H., Kinetically tuned dimensional augmentation as a versatile synthetic route towards robust metal-organic frameworks. *Nat. Commun.* **2014,** 5.